Chinese Chemical Letters 37 (2026) 111584

Contents lists available at ScienceDirect

Chinese Chemical Letters

journal homepage: www.elsevier.com/locate/cclet

Haploides A–G: Diterpenoids featuring four new carbon skeletons *via* non-carbocation-driven skeletal diversification

Ming-Zhu Zhu[a,d,1], Ze-Jun Xu[a,b,1], Jiao-Zhen Zhang[a], Li-Zhi Shi[a], Zong-Xu Gao[a], Yi Li[a], Shuang-Zhi Yuan[a], Yan-Rong Ma[a], Ai-Xia Cheng[a], Hong-Xiang Lou[a,b,c,*]

[a] *Department of Natural Products Chemistry, Key Lab of Chemical Biology (MOE), School of Pharmaceutical Sciences, Shandong University, Ji'nan 250012, China*
[b] *State Key Laboratory of Discovery and Utilization of Functional Components in Traditional Chinese Medicine, Shandong University, Ji'nan 250012, China*
[c] *Joint research institute of Medical and Pharmaceutical Sciences, Qilu Hospital, Shandong University, and Shandong Maternal and Child Care Hospital, Ji'nan 250012, China*
[d] *Department of Pharmacy, The Second Hospital, Cheeloo College of Medicine, Shandong University, Ji'nan 250033, China*

ARTICLE INFO

Article history:
Received 7 May 2025
Revised 8 July 2025
Accepted 11 July 2025
Available online 11 July 2025

Keywords:
Labdane diterpenoids
New carbon skeletons
Haplomitrium mnioides
Biosynthesis
Single-crystal X-ray diffraction
Anti-inflammatory activity

ABSTRACT

A series of highly rearranged labdane diterpenoids featuring previously unreported skeletons, including 9,18-cyclolabdanes (**1** and **2**), 1,10-*seco*-9,18-cyclolabdanes (**3–5**), 7,18-cyclolabdanes (**6**), and 1,10-*seco*-1,5-cyclolabdanes (**7**), along with seven novel labdanes (**8–14**), two novel halimane diterpenoids (**15** and **16**), and three known congeners (**17–19**), were isolated from Chinese liverwort *Haplomitrium mnioides*. Their structures were unequivocally determined through comprehensive spectroscopic analysis, single-crystal X-ray diffraction and electronic circular dichroism (ECD) calculations. These diverse diterpenoids were biosynthesized through an aldol-type cascade process, using **19** as the starting material, distinguishing them from compounds generated *via* conventional carbocation rearrangement. Anti-inflammatory assays revealed that haploide O (**15**) and haplomitrenolide C (**17**) significantly inhibited the secretion of proinflammatory cytokines interferon-γ (IFN-γ), tumor necrosis factor-α (TNF-α), and interleukin-6 (IL-6) *in vitro* in concanavalin A (ConA)-induced murine spleen cells.

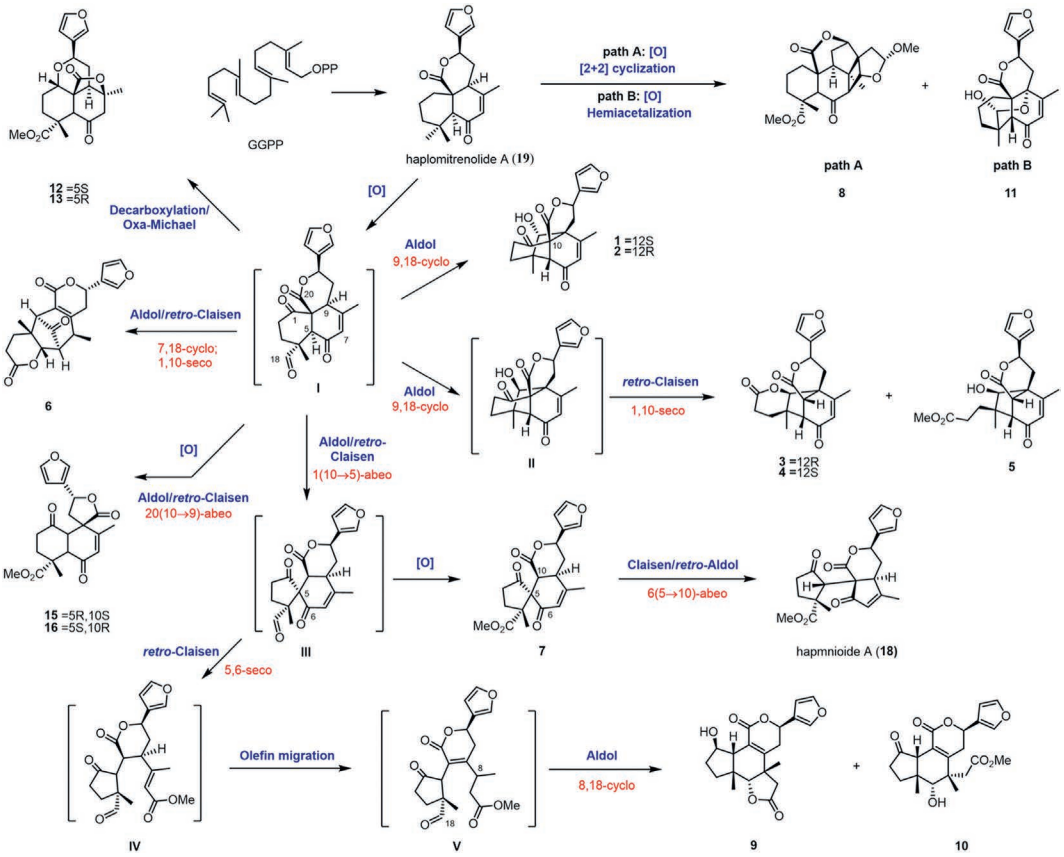
© 2026 Published by Elsevier B.V. on behalf of Chinese Chemical Society and Institute of Materia Medica, Chinese Academy of Medical Sciences.

Terpenoid natural products, characterized by stereochemically complex architectures, have long served as inspiration sources for therapeutic agent development [1,2]. Among diterpenoid derivatives, labdanes represent a structurally unique diterpenoid subclass encompassing pharmaceutically significant metabolites, including andrographolide, forskolin, and chlorolissoclimide. Labdane-type diterpenoids demonstrate remarkable structural plasticity through diverse skeletal rearrangements (Fig. S1 in Supporting information) [3,4]. Although carbocation-driven skeletal reorganizations represent well-characterized biochemical transformations in terpenoid biosynthesis [5–8], diversity-oriented transformations mediated by aldolase-type cascade mechanisms constitute an emerging area of research in natural product biogenesis, with limited characterized examples reported to date [9,10].

As ancient representatives of the embryophytic lineage, liverworts occupy a phylogenetically pivotal position as the earliest-diverging land plants. This taxonomically rich division, consisting of over 23,000 taxonomically validated species globally, represents a prolific source of structurally diverse specialized metabolites, particularly bisbibenzyls and terpenoids [11–19]. Notably, labdane-derived *Haplomitrium* diterpenoids are isolated exclusively from the genus *Haplomitrium* and have been identified as chemical markers for this liverwort lineage [18]. Our phytochemical exploration of Haplomitrium mnioides (Lindb.) R.M.Schust., collected from Xiangling Mountain within Ya'an City, Sichuan Province, China, yielded 19 diterpenoid derivatives, including 16 novel compounds designated haploides A–P (**1–16**). Structural characterization revealed four unprecedented carbon skeletons: 9,18-cyclolabdanes (**1** and **2**), 1,10-*seco*-9,18-cyclolabdanes (**3–5**), 7,18-cyclolabdanes (**6**), and 1,10-*seco*-1,5-cyclolabdanes (**7**). Seven additional labdanes (**8–14**) featuring our previously identified scaffolds [17,18], two labdane-related diterpenoids (**15** and **16**), and three known analogs (**17–19**) (Scheme 1), were isolated (Fig. 1). Moreover, four pairs of novel diastereomers, haploides A and B (**1** and **2**), C and D (**3** and **4**), L and M (**12** and **13**), and O and P (**15** and **16**) were simultaneously discovered. A plausible aldol-type cascade biogenetic pathway was deduced for the formation of these novel

* Corresponding author.
E-mail address: louhongxiang@sdu.edu.cn (H.-X. Lou).
[1] These authors contributed equally to this work.

https://doi.org/10.1016/j.cclet.2025.111584
1001-8417/© 2026 Published by Elsevier B.V. on behalf of Chinese Chemical Society and Institute of Materia Medica, Chinese Academy of Medical Sciences.



Scheme 1. Plausible biogenetic pathways for compounds **1**–**13**, **15**, **16**, **18**, **19**.

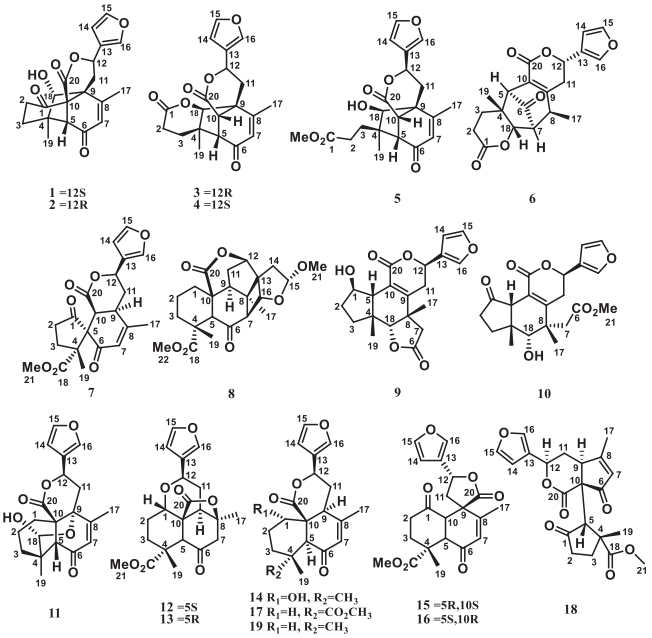


Fig. 1. Chemical structures of compounds **1**–**19**.

skeleton labdanes. Anti-inflammatory assays revealed that haploide O (**15**) and haplomitrenolide C (**17**) significantly inhibited the secretion of proinflammatory cytokines interferon-γ (IFN-γ), tumor necrosis factor-α (TNF-α), and interleukin-6 (IL-6). Herein, we report the isolation, structural characteristics, proposed biosynthetic pathways, and anti-inflammatory activity of these diterpenoids.

Haploide A (**1**) was obtained in the form of colorless crystals. High-resolution electrospray ionization mass spectrometry (HRESIMS) at *m/z* 379.1155 (calcd. for $C_{20}H_{20}O_6Na^+$ 379.1152) indicated that its molecular formula is $C_{20}H_{20}O_6$, indicating 11 indices of hydrogen deficiency. Nuclear magnetic resonance (NMR) spectra indicated the presence of two methyl groups [δ_H 2.27 (s), 1.00 (s)]; three methylenes; three methines, including two oxygenated methines [δ_H 5.67 (dd, J = 11.3, 6.2 Hz), δ_C 77.0; δ_H 4.29 (t, J = 2.2 Hz), δ_C 81.7]; three quaternary carbons; three carbon-carbon double bonds [δ_H 6.02 (s), 6.60 (brs), 7.50 (t, J = 1.6 Hz), 7.64 (brs); δ_C 128.7, 166.4, 126.2, 110.1, 144.9, 142.1], two keto carbonyls (δ_C 198.4, 207.5); and one ester carbonyl (δ_C 170.5). It was deduced that haploid A (**1**) contained five rings. The NMR data of **1** were similar to those of haplomitrenonolide A, except for the existence of a C−C bond between C-9 and C-18, one hydroxy group at C-18, and one keto carbonyl at C-1. These deductions were confirmed based on heteronuclear multiple bond correlations (HMBCs) from H_3–19 (δ_H 1.00) to C-3 (δ_C 37.0), C-4 (δ_C 45.9), C-5 (δ_C 61.7), and C-18 (δ_C 81.7); from H_3–17 (δ_H 2.27) to C-7 (δ_C 128.7), C-8 (δ_C 166.4), and C-9 (δ_C 57.4); from H-18 (δ_H 4.29) to C-3, C-5, C-8, and C-11 (δ_C 34.0); and from H_2–3 (δ_H 1.98) to C-1 (δ_C 207.5) (Fig. 2A). Thus, the planar structure for **1** was unequivocally confirmed as having a novel 9, 18-cyclolabdane skeleton.

Additionally, the signals of H-18/H_3–19, H_3–19/H-5, H-18/H_2–2, H-18/H_2–11, and H_3–17/H-12 in the nuclear Overhauser enhancement spectroscopy (NOESY) results indicated the cofacial nature of these protons (Fig. 2A). Ultimately, a single-crystal X-ray diffraction analysis, considering a Flack parameter of 0.00 (11) and using Cu Kα radiation (CCDC 2344630), finally established the absolute structure as 4*R*,5*R*,9*S*,10*R*,12*S*,18*S*. Haploide B (**2**) shared the same molecular formula and exhibited nearly identical NMR data as those of **1**, except for the chiral inversion at C-12, as af-

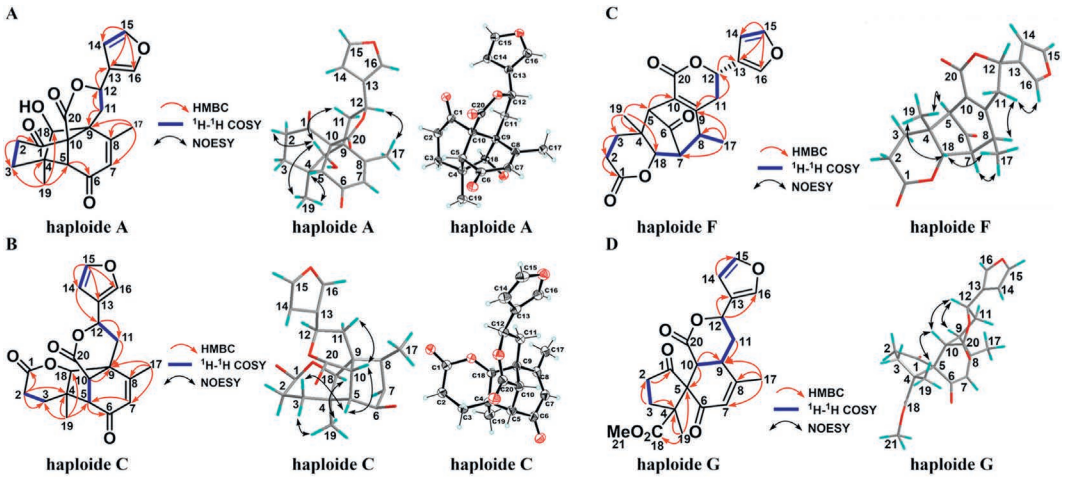


Fig. 2. Key ^{1}H−^{1}H COSY, HMBC, NOESY correlations of haploide A, C, F, G, and ORTEP drawings of haploides A, C.

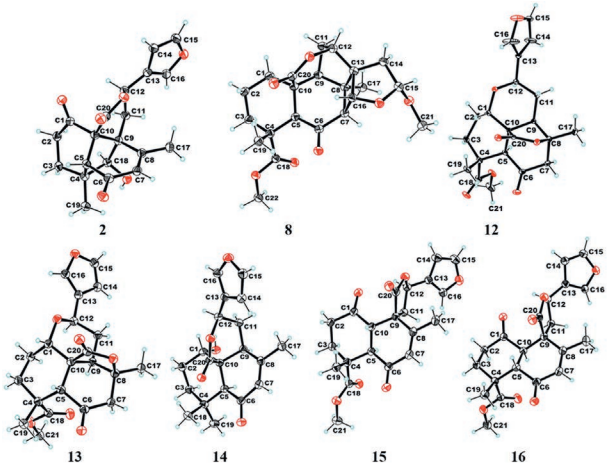


Fig. 3. X-ray crystallographic structure of compounds **2**, **8**, **12**–**16**.

firmed based on the NOESY signal of H_3–19/H-5, H-18/H_2–2, H-18/H_2–11, electronic circular dichroism (ECD) calculations (Fig. S2 in Supporting information), and X-ray diffraction (Cu Kα radiation, CCDC 2344631) (Fig. 3). Thus, haploide B (**2**) was determined to be the C-12 epimer of **1**, with an absolute configuration of 4*R*,5*R*,9*S*,10*R*,12*R*,18*S*.

Haploide C (**3**) was assigned the same molecular formula as that of haploide B (**2**). However, several structural differences were noted: The A-ring was cleaved between C-1 and C-10, and the lactone ring was formed between C-1 and C-18 in **3**, supported by HMBCs from H_2–2 (δ_H 2.39, 2.54) to C-1 (δ_C 171.1); from H_2–3 (δ_H 1.82, 2.22) to C-1; and from H-10 (δ_H 3.00) to C-4 (δ_C 43.3), C-5 (δ_C 59.9), C-8 (δ_C 163.2), C-9 (δ_C 54.0), C-18 (δ_C 88.7), and C-20 (δ_C 169.3); as well as the key ^{1}H–^{1}H correlation spectroscopy (COSY) correlations of H-5 (δ_H 3.36)/H-10 and H-10/H-18 (δ_H 4.15) (Fig. 2B). The relative configuration was inferred based on the NOESY correlations of H_3–19/H-18, H_3–19/H-3α, H-3β/H-5, H-5/H-10, and H-10/H-11β. Ultimately, the absolute structure of **3** was determined based on single-crystal X-ray diffraction using Cu Kα radiation (CCDC 2344632), indicating the absolute stereochemistry to be 4*R*,5*S*,9*S*,10*S*,12*R*,18*R*. Haploide D (**4**) was identified as the C-12 epimer of **3** based on their similar NMR spectrum and NOESY signals of H_3–19/H-18, H-10/H-12, H_3–19/H-3α, H-3β/H-5, H-5/H-10, and H-10/H-11β in **4**. The consistency of experimental and calculated CD curves (Fig. S2) determined the absolute configuration of **4** as 4*R*,5*S*,9*S*,10*S*,12*S*,18*R*.

Haploide E (**5**) had one fewer degree of unsaturation than **3**, and it has a similar planar structure to **3**, except for the lactone ring being cleaved between C-1 and C-18, and one carbomethoxy unit formed at C-1 in **5**. These deductions were supported by HMBCs from H_3–21 (δ_H 3.66) to C-1 (δ_C 174.4); and from H-18 (δ_H 4.26) to C-3 (δ_C 37.7), C-9 (δ_C 52.1), C-10 (δ_C 50.9), and C-11 (δ_C 30.9); along with the ^{1}H−^{1}H COSY signal of H-5 (δ_H 37.7)/H-10 (δ_H 37.7). The NOESY correlations of H_3–19/H-18, H-5/H-10, and H-10/H-11α determined the relative configuration of **5**. Comparing the experimental and calculated ECD data (Fig. S2), the absolute configuration of **5** was established as 4*R*,5*S*,9*S*,10*S*,12*R*,18*S*.

Haploide F (**6**) exhibited the same molecular formula as **4**. The NMR spectrum of **6** was extremely similar to that of **4**, except for the intramolecular cyclization between C-7 and C-18 in **6**, unlike that between C-9 and C-18 in **4**. Additionally, the double bond shifted from C_7–C_8 to C_9–C_{10} in **6.** These deductions were confirmed by HMBCs from H_3–17 (δ_H 1.59, d, J = 7.4 Hz) to C-7 (δ_C 55.6), C-8 (δ_C 46.2), and C-9 (δ_C 155.7); from H_2–11 (δ_H 2.58, 2.86) to C-9 and C-10 (δ_C 124.2); from H-5 (δ_H 3.30) to C-9 and C-10; from H-18 (δ_H 4.47) to C-7; and from H-7 (δ_H 2.95) to C-4 (δ_C 43.8) (Fig. 2C); as well as the ^{1}H–^{1}H COSY signals of H-8 (δ_H 3.28)/H-7 and H-7/H-19 (Fig. 2C). Thus, the planar structure for **6** was unequivocally clarified as a novel 7,18-cyclolabdane skeleton. The NOESY correlations of H_3–17/H-7, H-5/H_3–19, H_3–19/H-18, H-18/H_3–17, H-8/H-11β, and H-11β/H-16 suggested the relative configuration of **6**. From the perspective of the biogenic pathway, the structure of **6** was determined considering the absolute configuration of **4** and their similar ECD curves. Ultimately, ECD calculations (Fig. S2) identified the absolute configuration of the **6** as 4*R*,5*S*,7*S*,8*S*,12*S*,18*S*.

Haploide G (**7**) was determined to have the molecular formula $C_{21}H_{22}O_7$ *via* HRESIMS (*m/z* 409.1251 $[M+Na]^+$, calcd. 409.1258), with 11 degrees of unsaturation. ^{1}H and ^{13}C NMR spectra suggested its high similarity to haplomitrenolide C [20], except for the rearrangement of the A-ring from a six-membered to a five-membered carbon ring, connected to the B-ring at C-5 (δ_C 66.6), and introduction of one carbonyl group at C-1 (δ_C 213.3). These results were confirmed based on HMBCs from H_3–19 (δ_H 1.31) to C-3 (δ_C 32.0), C-4 (δ_C 56.1), C-5, and C-18 (δ_C 171.8); and from H-10 (δ_H 3.50) to C-1, C-5, and C-9; as well as the key ^{1}H–^{1}H COSY correlations of H-9/H-10. NOESY correlations of H_3–19/H-10, H-10/H-12, and H-12/H-9 (Fig. 2D) suggested two possible relative configurations for compound **7**, designated as **7** (4*R*,5*R*,9*R*,10*S*,12*R*)

and **7** (4*S*,5*S*,9*R*,10*S*,12*R*). ECD calculations were performed for both diastereomers, and the results revealed that the experimental ECD spectrum of compound **7** showed a better agreement with the calculated spectrum of **7** (4*R*,5*R*,9*R*,10*S*,12*R*) than that of **7** (4*S*,5*S*,9*R*,10*S*,12*R*) (Fig. S2). To further validate their configurations, seven low-energy conformers of compound **7** within 3.0 kcal/mol (Fig. S3 and Table S4 in Supporting information) with a specific gravity of Boltzmann distribution >1.0 % were refined and considered for density functional theory (DFT) and Gauge-Independent Atomic Orbital (GIAO) NMR shift calculation at the mPW1PW91/6–31G(d) level of theory [21,22]. The correlation coefficient was the key parameter applied for quantifying the agreement between the calculated and experimental ^{1}H and ^{13}C NMR data, and the results further supported the assignment of **7** (4*R*,5*R*,9*R*,10*S*,12*R*) (Fig. S4 in Supporting information). Ultimately, the absolute structure was determined as 4*R*,5*R*,9*R*,10*S*,12*R*.

The ^{1}H and ^{13}C NMR spectra of haploide H (**8**) were similar to those of haplomintrin A [17], except for the presence of one methoxy (δ_H 3.39; δ_C 55.1) and the absence of a double bond. HMBCs from H_3–21 (δ_H 3.39) to C-15 (δ_C 109.8); and from H-15 (δ_H 5.29) to C-14 (δ_C 37.3), C-21 (δ_C 55.1), C-13, and C-16; along with the ^{1}H–^{1}H COSY signals of H_2–14/H-15 suggested that the double bond at C-14 was reduced, and one methoxy was connected at C-15 in **8**. NOESY correlations of H_3–19/H-3β, H-3α/H-5, H-5/H-9, H-9/H_3–17, H_3–17/H-7, H-7/H_3–21, and H-7/H-16 indicated the relative configuration of **8**. Ultimately, the absolute structure of **8** was determined to be 4*R*,5*S*,7*S*,8*R*,9*S*,10*S*,12*R*,13*S*,15*R*,16*R*, based on the single-crystal X-ray diffraction analysis with Cu Kα radiation (CCDC 2344633) (Fig. 3).

Haploide I (**9**) was identified as the C-5 epimer of hapmnioide C [18], based on their similar NMR spectra and NOESY signals of H_3–17/H-18, H-18/H_3–19, H_3–19/H-5, H-18/H-3β, H-3α/H-1, H_3–17/H-11β, and H-11β/H-14. The absolute configuration of **9** was confirmed to be 1*R*,4*R*,5*S*,8*S*,12*R*,18*R* based on ECD calculations (Fig. S2). The NMR data of haploide J (**10**) suggested a similar planar structure to that of **9**. However, the five-membered lactone ring was hydrolyzed, and the carboxyl group at C-6 underwent esterification, thereby introducing a methyl ester group. Additionally, the hydroxyl group at C-1 was oxidized to the carbonyl group in **10**. These predictions were determined based on the HMBC signals from H_3–21 (δ_H 3.62) to C-6 (δ_C 171.2), from H_2–7 (δ_H 2.43, 2.83) to C-6, from H_2–2 (δ_H 2.31, 2.49) to C-1 (δ_C 215.7). The relative configuration of **10** was confirmed based on the NOESY signals of H_3–17/H-18, H-18/H_3–19, H_3–19/H-5, H_3–17/H-11β, and H-11β/H-14. Accordingly, the configuration of **10** was determined to be 4*R*,5*S*,8*S*,12*R*,18*R* based on the ECD calculations (Fig. S2) and biosynthetic pathways.

Haploide K (**11**) showed one fewer degree of unsaturation than **2**, and its NMR data were similar to those of **2**, except for the presence of one hemiacetal signal (δ_H 4.70; δ_C 97.1) and the absence of the ketone group. HMBCs from H_3–19 to C-3, C-4, C-5, and C-18 (δ_C 97.1); from H_3–17 to C-7, C-8, and C-9 (δ_C 75.5); along with the key ^{1}H–^{1}H COSY signal of H_2–1 (δ_H 1.73)/H_2–2, suggested that the ketone at C-1 was reduced, and epoxidation occurred between C-9 and C-19, unlike **2**. The relative configuration of **11** was established based on the NOESY correlations of H-5/H_3–19, H_3–19/H-18, and H-1/H-12. Comparing the experimental and calculated ECD curves (Fig. S2), the absolute configuration of **11** was determined to be 4*R*,5*R*,9*S*,10*R*,12*R*,18*R*.

Haploides L and M (**12** and **13**) were identified as a pair of C-5 epimers, sharing the same molecular formula of $C_{21}H_{24}O_7$. The NMR spectra of **12** closely resembled those of cacofuran B [23], except for the presence of one keto carbonyl at C-6 (δ_C 203.4), two ester carbonyls at C-18 (δ_C 177.7) and C-20 (δ_C 177.0), one oxygenated methine at C-1 (δ_C 65.2), one oxygenated methyl attached to C-18, and one ether bond between C-1 and C-12, as confirmed by HMBCs from H-12 (δ_H 4.99) to C-1; from H-1 (δ_H 3.86) to C-12; from H_3–19 (δ_H 1.26) to C-3 (δ_C 31.7), C-4 (δ_C 42.4), C-5 (δ_C 59.3), and C-18 (δ_C 177.7); from H_3–21 (δ_H 3.70) to C-18; and from H-5 (δ_H 3.68) to C-6 (δ_C 203.4) and C-20 (δ_C 177.0). Its relative configuration was determined based on the NOESY signals of H_3–19/H-3β, H-3β/H-1, H-3α/H-5, H-5/H-9, H-9/H_3–17, H-9/H-12. The absolute configuration (1*S*,4*R*,5*S*,8*S*,9*R*,10*S*,12*R*) of **12** was conclusively determined by combining X-ray diffraction results (Cu Kα radiation, CCDC 2344628) (Fig. 3). The NOESY signals (H_3–19/H-5, H-5/H-3β, H-3β/H-1, H-9/H_3–17, H-9/H-12) of **13** indicated that it represents the C-5 epimer of **12**. Finally, the absolute configuration of **13** was determined as 1*S*,4*R*,5*R*,8*S*,9*R*,10*S*,12*R* by single-crystal X-ray diffraction using Cu Kα radiation (CCDC 2344629) (Fig. 3).

The NMR data of **14** closely resembled those of **19** [20], with the only difference being the chemical shift at C-1 (δ_C 34.2 in **19** *vs.* δ_C 66.5 in **14**), revealing the presence of a hydroxyl group at this position. This was supported by the ^{1}H–^{1}H COSY signals of H-1 (δ_H 4.43)/H-2 (δ_H 1.74, 1.91). The relative configuration of **14** was determined based on the NOESY signals of H-5/H-9, H-11β/H-1, H-1/H-12, and H-14/H_3–17. Ultimately, the absolute structure of **14** was determined to be 1*S*,5*S*,9*S*,10*S*,12*R* based on the single-crystal X-ray diffraction using Cu Kα radiation (CCDC 2344634) (Fig. 3).

Haploides O and P (**15** and **16**) were identified as a pair of C-5 and C-10 isomers based on their identical molecular formula of $C_{21}H_{22}O_7$. The NMR data of **15** suggested that its planar structure was similar to that of haplomitrenolide C [20], except that the six-membered lactone ring was replaced by a five-membered lactone ring that was connected to the B-ring by spiroC-9, and one ketone was introduced at C-1 (δ_C 207.3). These deductions were confirmed by key HMBCs from H_3–17 to C-9 (δ_C 51.0); from H_2–2 to C-1; from H-10 to C-9; from H_2–11 to C-9, C-12, C-13, and C-20; from H-12 to C-9, C-11, and C-13; along with the ^{1}H–^{1}H COSY signals of H_2–11/H-12. The relative configuration of haploide O (**15**) was deduced from NOESY correlations of H-5/H_2–11 and H-10/H_3–19. The absolute structure of haploide O (**15**) was finally confirmed to be 4*R*,5*R*,9*R*,10*S*,12*R* through single-crystal X-ray diffraction using Cu Kα radiation (CCDC 2344624) (Fig. 3). Moreover, the absolute structure of haploide P (**16**) was established as 4*R*,5*S*,9*R*,10*R*,12*R*, according to the NOESY correlations (H_3–19/H-5 and H_2–11/H-10) and Cu Kα single-crystal X-ray diffraction analysis (CCDC 2344625) (Fig. 3).

A biogenetic network was postulated for **1–19**, rationalizing their skeletal diversification through aldol-type cascade transformations (Scheme 1). The biosynthetic origin can be traced to **19**, which is derived from geranylfarnesyl pyrophosphate *via* a series of enzymatic reactions and then undergoes oxidization/[2 + 2] cyclization or oxidization/hemiacetalization to afford **8** and **11**, respectively. Central to this network is the C-1 oxidation event, which generates key intermediate **I**. Regioselective aldolase-mediated aldol/*retro*-Claisen rearrangements at divergent positions of intermediate **I** account for the structural divergence observed in compounds **1–7**. Specifically, C9-specific aldol/*retro*-Claisen transformations of intermediate **I** produce the labdane-derived derivatives **15** and **16**. Structural elaboration of **7** through Claisen/*retro*-aldol reactivity at the C10-adjacent ester moiety culminates in the formation of **18**. For **9** and **10**, intermediate **III** undergoes a tandem sequence cascade involving *retro*-Claisen cleavage, olefinic double-bond migration, and subsequent Claisen-type reorganization at C8 to establish their characteristic frameworks.

All isolated compounds were systematically screened for their anti-inflammatory potential, focusing on their ability to modulate the secretion of key proinflammatory cytokines. Given the pivotal role of proinflammatory cytokines, such as IFN-γ, TNF-α, and IL-6, in mediating inflammatory responses through immune cell activation and tissue damage amplification [24], the anti-inflammatory efficacy of the compounds was evaluated by measuring their ability

to suppress these cytokines in ConA-induced murine spleen cells. Notably, haploide O (**15**) and haplomitrenolide C (**17**) demonstrated significant anti-inflammatory activity, effectively inhibiting the secretion of these proinflammatory cytokines at a concentration of 10 μmol/L (Fig. S15 in Supporting information). These findings highlight the therapeutic potential of these compounds in mitigating inflammatory responses.

In conclusion, four unprecedented labdane scaffolds were isolated and identified from *H. mnioides*: 9,18-cyclolabdanes (**1** and **2**), 1,10-*seco*-9,18-cyclolabdanes (**3–5**), 7,18-cyclolabdanes (**6**), and 1,10-*seco*-1,5-cyclolabdanes (**7**), along with seven novel labdanes (**8–14**), two novel halimane diterpenoids (**15** and **16**), and three known congeners (**17**–**19**). Interestingly, four pairs of novel diastereomers, haploides A and B (**1** and **2**), C and D (**3** and **4**), L and M (**12** and **13**), and O and P (**15** and **16**) were simultaneously isolated. In addition, the plausible biosynthetic pathways of compounds **1**–**18** were deduced to originate from **19** as the starting material through an aldol-type cascade process. Anti-inflammatory assays revealed that haploide O (**15**) and haplomitrenolide C (**17**) significantly inhibited the secretion of the proinflammatory cytokines IFN-γ, TNF-α, and IL-6 in ConA-induced murine spleen cells. These findings provide valuable insights into the chemical diversity and biological activity of labdane diterpenoids.

Declaration of competing interest

The authors declare that they have no known competing financial interests or personal relationships that could have appeared to influence the work reported in this paper.

CRediT authorship contribution statement

Ming-Zhu Zhu: Writing – original draft, Methodology, Investigation, Formal analysis, Data curation. **Ze-Jun Xu:** Writing – review & editing, Supervision, Investigation, Formal analysis. **Jiao-Zhen Zhang:** Investigation, Formal analysis. **Li-Zhi Shi:** Investigation. **Zong-Xu Gao:** Investigation. **Yi Li:** Investigation. **Shuang-Zhi Yuan:** Investigation. **Yan-Rong Ma:** Investigation. **Ai-Xia Cheng:** Investigation. **Hong-Xiang Lou:** Writing – review & editing, Supervision, Project administration, Methodology, Investigation, Funding acquisition, Formal analysis, Data curation.

Acknowledgments

Financial support was provided by the National Natural Science Foundation of China (Nos. 82293682, 82173703, and 82273807), and Shandong Provincial Natural Science Foundation (No. ZR2022YQ74).

Supplementary materials

Supplementary material associated with this article can be found, in the online version, at doi:10.1016/j.cclet.2025.111584.

References

[1] T. Rodrigues, D. Reker, P. Schneider, G. Schneider, Nat. Chem. 8 (2016) 531–541.
[2] Y.J. Wang, P. Tang, W.C. Tu, et al., Chin. Chem. Lett. 36 (2025) 109955.
[3] L. Xiong, Q.M. Zhou, Y.K. Zou, et al., Org. Lett. 17 (2015) 6238–6241.
[4] O. Antoniuk, A. Maranha, J.A.R. Salvador, et al., Nat. Prod. Rep. 41 (2024) 1858–1894.
[5] D.J. Tantillo, Nat. Prod. Rep. 28 (2011) 1035–1053.
[6] A. Minami, T. Ozaki, C. Liu, et al., Nat. Prod. Rep. 35 (2018) 1330–1346.
[7] P. Luo, J.M. Lv, H.T. Zhen, et al., Chin. Chem. Lett. 36 (2025) 111042.
[8] G.B. Tabekoueng, H. Li, B. Goldfuss, et al., Angew. Chem. Int. Ed. 63 (2024) e202413860.
[9] C. Zeymer, R. Zschoche, D. Hilvert, J. Am. Chem. Soc. 139 (2017) 12541–12549.
[10] Li Y.Q, M.J. Cong, W.G. Wang, et al., Angew. Chem. Int. Ed. 63 (2024) e202403365.
[11] H.D. Zinsmeister, H. Becker, T. Eicher, Angew. Chem. Int. Ed. 30 (1991) 130–147.
[12] T. Shen, X.N. Wang, H.X. Lou, Nat. Prod. Rep. 26 (2009) 916–935.
[13] J.B. Qu, L.M. Sun, H.X. Lou, Chin. Chem. Lett. 24 (2013) 801–803.
[14] M. Rempt, G. Pohnert, Angew. Chem. Int. Ed. 49 (2010) 4755–4758.
[15] L.N. Wang, J.Z. Zhang, X. Li, et al., Org. Lett. 14 (2012) 1102–1105.
[16] J.Z. Zhang, R.X. Zhu, G. Li, et al., Org. Lett. 14 (2012) 5624–5627.
[17] J.C. Zhou, J.Z. Zhang, A.X. Cheng, et al., Org. Lett. 17 (2015) 3560–3563.
[18] J.C. Zhou, J.Z. Zhang, R.J. Li, et al., Org. Lett. 18 (2016) 4274–4276.
[19] Y. Li, Z.J. Xu, R.X. Zhu, et al., Org. Lett. 22 (2020) 510–514.
[20] Y. Asakawa, M. Toyota, T. Masuya, Phytochemistry 29 (1990) 585–589.
[21] L. Grauso, R. Teta, G. Esposito, et al., Nat. Prod. Rep. 36 (2019) 1005–1030.
[22] X.X. Li, J. Fu, Y.H. Li, et al., Org. Lett. 24 (2022) 1388–1393.
[23] J. Tanaka, G. Marriott, T. Higa, et al., J. Nat. Prod. 64 (2001) 1468–1470.
[24] M.F. Neurath, Nat. Rev. Immunol. 24 (2024) 559–576.